International Journal of Nanoelectronics and Materials
Volume 16, No. 4, October 2023 [843-852]

Hydrothermal Growth Zinc Oxide Nanorods for pH Sensor Application

K.L. Foo[1*], S.J. Tan[2, 3], C.Y. Heah[2, 3], Subash C.B. Gopinath[1, 4], Y.M. Liew[2, 4], U. Hashim[1] and C.H. Voon[1]

[1]Institute of Nano Electronic Engineering (INEE), Universiti Malaysia Perlis (UniMAP), 01000 Kangar, Perlis, Malaysia.
[2]Geopolymer and Green Technology, Centre of Excellence (CEGeoGTech), Universiti Malaysia Perlis (UniMAP), 01000 Perlis, Malaysia.
[3]Faculty of Mechanical Engineering Technology, Universiti Malaysia Perlis (UniMAP), 01000 Perlis, Malaysia.
[4]Faculty of Chemical Engineering Technology, Universiti Malaysia Perlis (UniMAP), 01000 Perlis, Malaysia.

Received 8 September 2022, Revised 13 September 2022, Accepted 20 September 2022

ABSTRACT

The aim of this work is to apply synthesized zinc oxide (ZnO) Nanorods using hydrothermal (HTL) growth technique for pH sensor application. The highly crystallite of ZnO Nanorods was obtained by anneal the growth ZnO Nanorods in furnace at 200 °C for 2 hours. Besides that, XRD analysis shows the produced ZnO Nanorods belonged to the (002) plane. Furthermore, Scanning Electron Microscope (SEM) images confirm that the ZnO Nanorods with hexagonal-faceted structural were successfully produced by HTL growth technique. In addition, Ultraviolet–visible (UV-Vis) spectrophotometer analysis shows that the synthesized ZnO belongs to the wide band gap semiconductor material. The growing ZnO Nanorods were then subjected to electrical measurement with various pH levels. The outcome demonstrates that the current rises as the solution changes from acidic to alkaline. Overall, our study shows a relationship between the electrical as well as the structural characteristics of ZnO Nanorods at various pH levels.

Keywords: Zinc Oxide Nanorods, hydrothermal growth, pH sensor, Interdigitated Electrodes.

1. INTRODUCTION

The exploration and development of nanostructure materials that result in high performance nanomaterial has contribute to the advancement of several chemical methods on a laboratory scale. Currently, there are several nanomaterials that have been extensively studied by researchers around the world, such as ZnO, Iron(III) oxide (Fe_2O_3), Titanium dioxide (TiO_2), Tin(IV) oxide (SnO_2), Indium(III) oxide (In_2O_3), Cobalt(II,III) oxide (Co_3O_4), and Copper(II) oxide (CuO). Among these materials, ZnO has some advantages over other nanomaterials-based sensors, such as its low cost and nontoxic nature, making it environmentally friendly. By the way, there are various methods to grow ZnO, such as electrodeposition [1], sol-gel [2], spray pyrolysis [3, 4], ink-jet printing [5], chemical vapour deposition [6] and sputtering [7]. In this project, the low-cos sol-gel approach has been chosen from among them. Sol-gel is a group under the chemical route deposition technique, whereby chemical route or solution-based route technique is widely used for the deposition of the ZnO. This technique usually involves the chemical reaction of zinc precursor such as zinc nitrate, and zinc chloride and zinc acetate with the reducing agent such as alcohol, sodium, ammonium carbonates, ammonium nitrates, and ammonium hydroxide along with the presence of precursor, such as monoethanolamine (MEA), diethanolamine (DEA), triethanolamine (TEA) and lattice acid.

* Corresponding author: klfoo@unimap.edu.my

In addition, there are also various methods have been used to grow ZnO Nanorods, such as HTL growth [8], vapor phase transport [9], metal-organic chemical vapor deposition [10], and vapor–liquid-solid (VLS) method [11]. While among these methods, the HTL method, which is classified under the liquid phase growth, has been chosen in this project. Whereby, the term HTL in this method implies a water pressure and a range of high temperatures. This method is preferred when growing ZnO Nanorods because it is a low-cost and simple process with high yield at low temperature and pressure.

Miniaturized sensors with organic sensitive membranes have been developed extensively in recent years for quality control in the food, safety, agricultural, military, monitoring, and particularly medical industries. The pH sensors have drawn a lot of research attention as biosensor platforms because of the similarities between ionic interactions in lab-on-a-chip technology. Besides, the food sector, the environment, and clinical safety all require pH testing for various control operations. By the way, the amount of hydrogen ions (H+) in a solution determines whether it is basic or acidic. Therefore, several pH buffer solutions were examined in this work employing interdigitated electrodes (IDEs) covered with ZnO Nanorods in order to detect acidic or basic solutions.

2. MATERIAL AND METHODS

2.1 Preparation of Zinc Oxide Thin films

In the ZnO solution preparation process, zinc acetate dehydrate (ZAD, $Zn(CH_2COO)_2{\cdot}2H_2O$), monoethanolamine (MEA) and 2-methoxyethanol (2ME, $CH_3O(CH_2)_2OH$) were utilized as starting material, stabilizer and solvent, respectively. The concentration of the mixture was prepared at 0.5 M and stirred using magnetic stirrer hotplate. Briefly, the process was started with a mixture of ZAD and 2-ME at 60 °C using a magnetic stirrer hotplate. After 30 minutes, MEA was added every 10 minutes for 2 hours while the mixture was continuously stirred on the magnetic stirrer hotplate at 60 °C. In order to produce a homogeneous and transparent solution, the resulting mixture was agitated for an additional 90 minutes. ZAD to MEA was fixed at a 1:1 molar ratio. Finally, the produced solution was kept for 24 hours at room temperature (RT).

2.2 Interdigitated Electrodes (IDE) Fabrication Process

In IDE fabrication process, a 4-inch silicon wafer substrate was first cleaned with standard cleaning procedure to remove organic residues and native oxide on the substrate. Next, wet oxidation process has been applied to grow a silicon oxide layer on the substrate with 300 nm thickness. Then, physical vapor deposition (PVD) process was performed to deposit a silver layer on top of the oxide layer. The sample was then undergone photolithography process by depositing photoresist using spin coat method at 3000 rpm for 20 s. The sample is then undergone soft bake process for 60 seconds at temperature of 90 °C on a hotplate. Next, the sample was exposed to ultraviolet (UV) light with IDE masks for 10 seconds to get desired pattern on the wafer. After patterning process, the wafer was immersed in resist developer to remove the softened photoresist layer. Then, hard bake process was performed for 60s at 90 °C to improve adhesion between photoresist and silver layer. Then, silver etchant was used to etch the uncovered silver layer with photoresist. After that, the resist was stripped using acetone and finally spin-dried using spin coater. The process flow for IDE fabrication process and design of IDE are shown in Figure 2. ZnO Nanorods based IDE fabrication process flow and Figure 3, respectively.

2.3 ZnO Nanorods Formation

The produced ZnO solution was spin coated on the IDE using the spin coat method with a spin speed of 3000 rpm for 20 s prior to the development process of ZnO Nanorods. The coated ZnO thin films were then dried on a hotplate for 10 minutes at 150 °C. To achieve the necessary thickness, this coating and drying process was done five times. After that, a typical muffle furnace was used to anneal the coated ZnO thin films at 200 °C for two hours, producing a highly crystalline ZnO seed layer. After the development of ZnO seed layer, ZnO Nanorods were produced utilizing HTL growth method. In this method, deionized water (DIW) was mixed with zinc nitride hexahydrate ($Zn(NO_3)_2$) and hexamethylenetetramine (HMT). A magnetic stirrer was used to agitate the combined solution for 20 minutes at RT. $Zn(NO_3)_2$ and HMT were kept in a 1:1 molar ratio, and the mixture's concentration was held at 0.035 M. The coated ZnO seed layer was submerged upside down in the ready-made stock solution for the growing process of the ZnO Nanorods after the $Zn(NO_3)_2$ and HMT powder were dissolved in the DIW. In a vacuum oven, the solution was heated up at 93 °C for six hours. After that, the growing process was completed, the samples' surfaces were cleaned by rinsing them in DIW to get rid of any remaining salt. To obtain extremely crystalline ZnO Nanorods, the growing ZnO Nanorods were annealed at 200 °C for 2 hours in a muffle furnace. Finally, using a conventional photolithography method, the design from the photomask for pad formation was transferred onto the substrates. Figure 1 depicts the process flow for the growth of ZnO Nanorods.

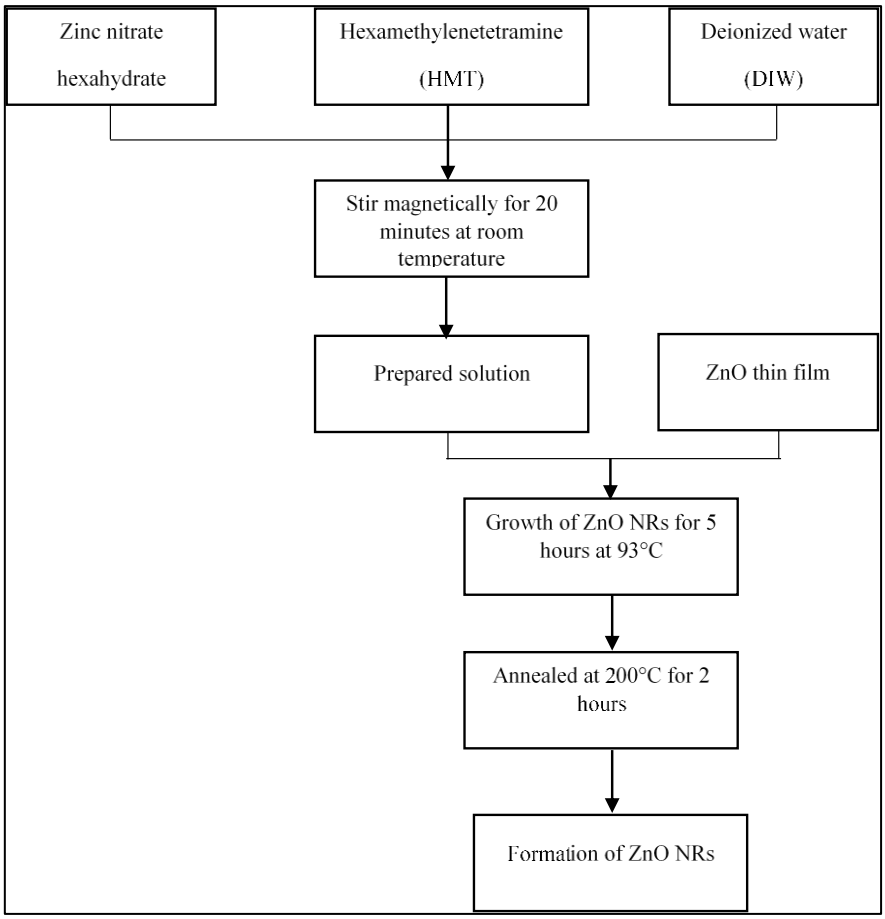

Figure 1. ZnO Nanorods growing process.

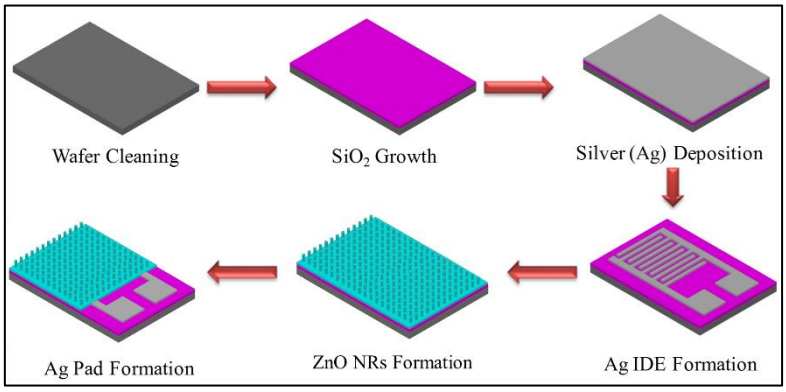

Figure 2. ZnO Nanorods based IDE fabrication process flow.

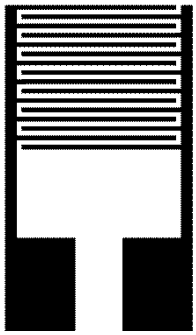

Figure 3: Design Of IDE.

2.4 Structural and electrical characterization

The surface analysis of ZnO Nanorods was investigated using scanning electron microscopy (Jeol JSM-6510) (SEM) for structural investigation. By using X-ray diffraction (Bruker D8, Bruker AXS, Inc., Madison, WI, USA) (XRD) with *Cu K* radiation (λ = 1.54), the crystallization of ZnO Nanorods was examined. In addition, a UV-Vis spectrophotometer (Perkin Elmer, Lambda 950) (UV-Vis) investigation of the optical characteristics and bandgap of the ZnO Nanorods at RT was conducted. Additionally, a current-voltage (I-V) curve was studied utilizing a two-point probe connected with a picoammeter (Keithley 6487) to examine the electrical characteristics of the ZnO Nanorods in various pH solutions.

3. RESULTS AND DISCUSSION

3.1 Scanning Electron Microscope (SEM)

The surface or structural characterization of the ZnO Nanorods was analyzed using SEM. The SEM pictures of produced ZnO Nanorods that were synthesis via HTL method are shown in Figure 4. From the SEM results, it demonstrates that the entire electrode surface has been covered by ZnO Nanorods. The Nanorods grew into an even and almost straight structure. This was due to the evenly deposition of the seed layer of ZnO thin films via sol-gel spin coating process. Besides that, the use of 2-ME as a solvent in seed solution preparation has resulted in a diameter about 200 nm. Furthermore, the top-view of zinc oxide Nanorods at 50 kX magnification shows a hexagonal-faceted morphology [12] as shown in Figure 4 (b), which proved the existence and growth of ZnO Nanorods.

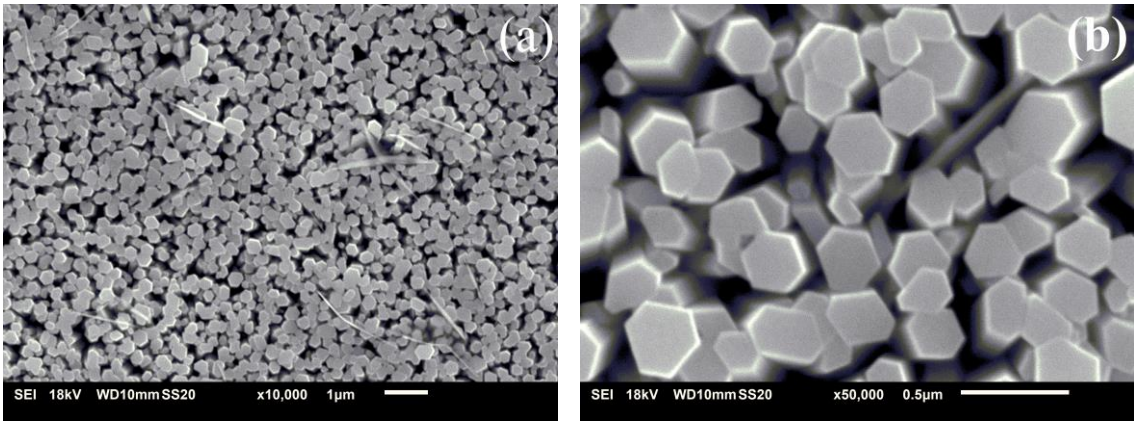

Figure 4. Top view SEM of ZnO Nanorods (a) 10 kX and (b) 50 kX.

3.2 X-ray diffraction (XRD)

XRD has been conducted to study the crystallographic orientation and crystallinity of HTL growth ZnO Nanorods. Figure 5 displays all the diffraction peaks that correspond to the standard card (JCPDS 36-1451). The sharp and narrow diffraction peaks in Figure 5 indicates that the HTL growth ZnO Nanorods exhibit high crystallinity. Additionally, the highest XRD peak at 34.6 º shows that the ZnO Nanorods prefer to grow along (002) planes in their crystal structure. According to M. Hessien et al's research, this nanostructure is polycrystalline with a hexagonal wurtzite structure because of the ZnO Nanorods' preferential crystal growth orientation at (002) planes [13]. Furthermore, this hexagonal wurtzite structure is clearly proved by the SEM image shown in Figure 4.

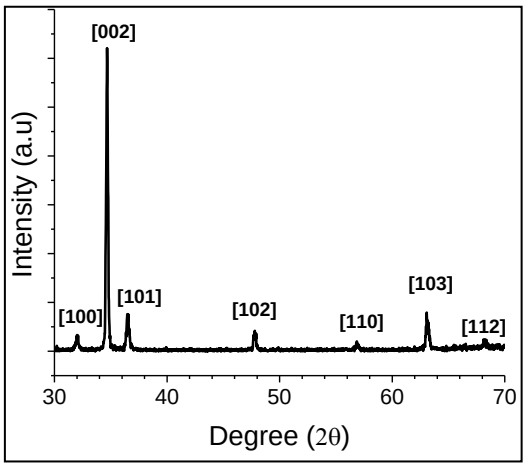

Figure 5. X-ray diffraction pattern of ZnO Nanorods.

3.3 Ultraviolet–Visible (UV-Vis) Spectroscopy

As illustrated in Figure 6, the optical characteristics of the HTL produced ZnO Nanorods were examined using UV-Vis spectroscopy. The transmittance of ZnO Nanorods at room temperature was determined in the wavelength range of 300–800 nm. In the UV zone, at wavelengths around 385 nm, the transmittance significantly decreases, as shown in Figure 6. This might be duo to the ZnO Nanorods have a strong absorption edge at 385 nm wavelengths. Tauc graphs [14], which represent the curve of $(\alpha hv)^2$ vs. photo-energy (hv), were plotted to determine the direct

bandgap for ZnO Nanorods, where is the absorption coefficient for the direct transition of ZnO and was determined by [15]:

$$\alpha = \frac{\ln(1/T)}{d} \tag{1}$$

where d stands for the ZnO thickness and T is the ZnO Nanorods' transmittance. On the other hand, the equation (2) can be used to determine how the optical band gap *(αhv)* at RT depends on the absorption coefficient (α) in the energy range of 3-3.5 eV [16]:

$$\alpha hv = B\left(hv - E_g\right)^n \tag{2}$$

where *n* represent the permitted direct band (½), *B* is the constant, *hv* represent photon energy and E_g is the band gap energy. Figure 7 illustrates how the intersection of the tangent to the linear portion of the curve and the *hv*-axis can be used to determine the direct bandgap of ZnO Nanorods. According to the Tauc graph in Figure 7, the bandgap of ZnO Nanorods synthesized using 2-ME solvent is 3.18 eV, which is near to the direct band-gap of ZnO (3.3 eV) [17].

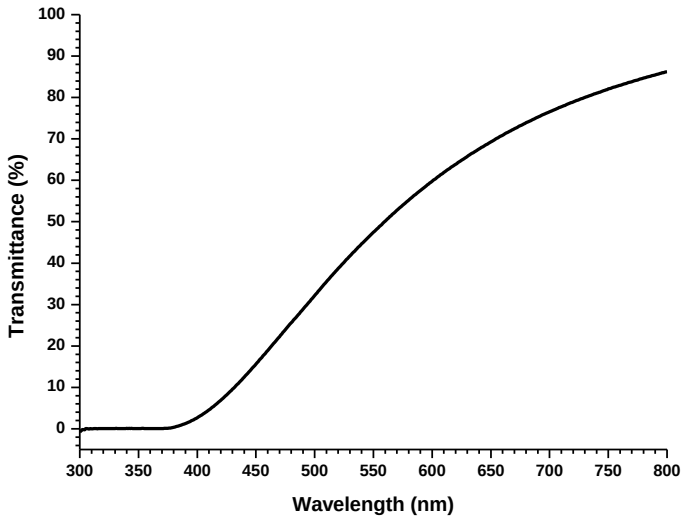

Figure 6. Optical properties of HTL growth ZnO Nanorods.

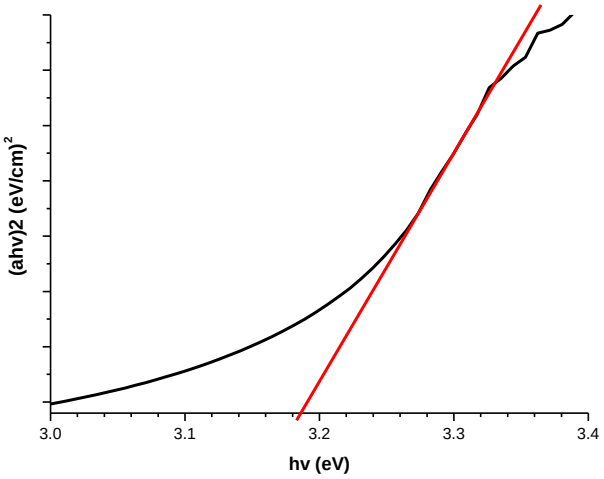

Figure 7. Plot of $(\alpha hv)^2$ vs. the photon energy for ZnO Nanorods

3.4 Electrical Properties of Zno Nanorods at Different pH Solution.

The current-voltage (I-V) characterization of ZnO Nanorods based IDE was conducted by connecting two-point probes using picoammeter. This analysis was carried out using various pH ranging from pH 4 to pH 12. The current was measured by applying the voltage from 0 V to 5 V. The result shown in Figure 8 clearly indicated that the ZnO Nanorods based IDE acted like an ohmic contact, which was a non-rectifying junction, where the I-V characteristic shows a nearly linear graph. On the other hand, the current values at 5 V were ranged from 1.69 nA to 23.7 nA. The graph shows the lowest current (1.69 nA) with pH 4 solution, while the highest current (23.7 nA) in pH 12 solution. In addition, results shown in Figure 9 could be clearly seen that the current of the ZnO Nanorods based IDE was increased with pH value. In other words, the conductivity of the sample was increased as the pH value approaches the alkaline solution. This is due to the alkaline solution presence more hydroxide ions (OH^-) if compared to the acidic solution and thus showing the increase of negative charges ion in alkaline solution.

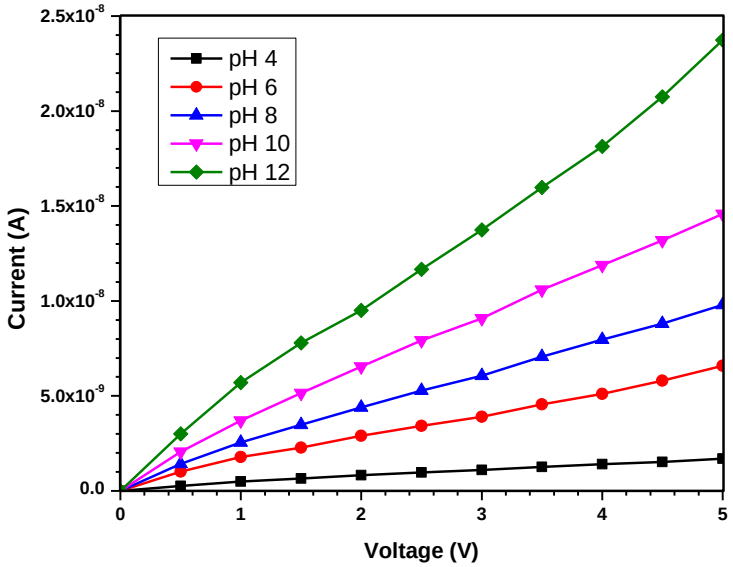

Figure 8. I-V characteristic for the ZnO Nanorods based IDE with various pH solution.

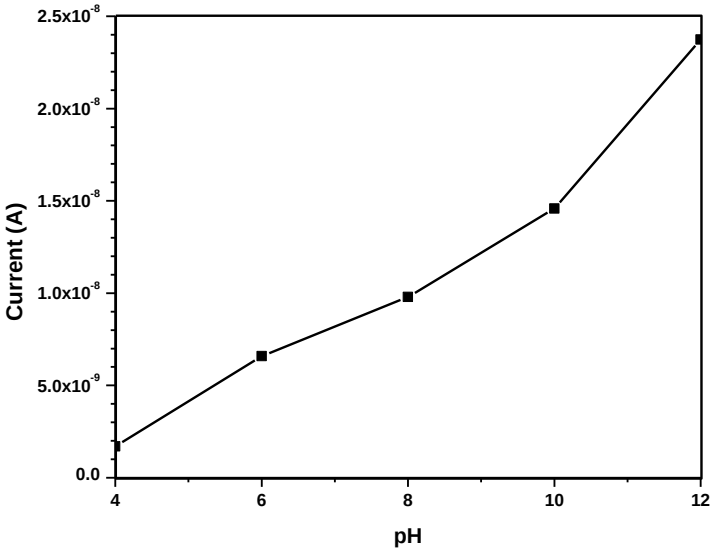

Figure 9. The current flow of ZnO Nanorods based IDE in different pH solution at 5 V.

4. CONCLUSION

The ZnO Nanorods were successfully synthesized through the HTL growth technique. The SEM analysis indicated that highly oriented hexagonal wurtzite structure ZnO Nanorods were successfully growth on the uniformly coated ZnO seed layer. The optical properties of the ZnO Nanorods show that the band-gap (3.18 eV) of the synthesized ZnO Nanorods using 2-ME solvent is close to 3.3 eV, which is the intrinsic band-gap of ZnO. Besides, the electrical properties indicate the highest current of 23.7 nA in the ZnO NR when pH 12 solution was tested. Therefore, it can be concluded that the conductivity of ZnO Nanorods increases when a more alkaline solution is used.

REFERENCES

[1] Oliveira, F. F., Proenca, M. P., Araújo, J. P. and Ventura, J., Journal of Materials Science vol **51**,issue 12 (2016) pp. 5589-5597
[2] Foo, K. L., Liu, W. W., Hashim, U. and Voon, C. H., "Fabrication and characterization of ZnO thin film on interdigitated electrode by sol-gel spin coating method for DNA detection," in 2014 IEEE Conference on Biomedical Engineering and Sciences (IECBES), (2014) pp. 489-492
[3] Ambedkar, A. K., Singh, M., Kumar, V., Kumar, V., Singh, B. P., Kumar, A. and Gautam, Y. K., Surfaces and Interfaces vol **19**,issue (2020) pp. 100504
[4] Roguai, S. and Djelloul, A., Applied Physics A vol **126**,issue 2 (2020) pp. 122
[5] Huang, L., Chen, F., Paydar, S. and Wu, Y., JOM vol **73**,issue 1 (2021) pp. 387-394
[6] Jones, A., Mistry, K., Kao, M., Shahin, A., Yavuz, M. and Musselman, K. P., Scientific Reports vol **10**,issue 1 (2020) pp. 19947
[7] Gonçalves, R. S., Barrozo, P., Brito, G. L., Viana, B. C. and Cunha, F., Thin Solid Films vol **661**,issue (2018) pp. 40-45
[8] Kashif, M., Hashim, U., Ali, M. E., Foo, K. L. and Usman Ali, S. M., Journal of Nanomaterials vol **2013**,issue (2013) pp. 478942
[9] Kumar, D. R., Ranjith, K. S., Nivedita, L. R. and Kumar, R. T. R., Journal of Rare Earths vol **35**,issue 10 (2017) pp. 1002-1007

[10] Manzoor, Z., Saravade, V., Corda, A. M., Ferguson, I. and Lu, N., ES Materials & Manufacturing vol **8**,issue (2020) pp. 31-35
[11] Yao, Y.-F., Chou, K.-P., Lin, H.-H., Chen, C.-C., Kiang, Y.-W. and Yang, C. C., ACS Applied Materials & Interfaces vol **10**,issue 47 (2018) pp. 40764-40772
[12] Jayalakshmi, G. and Saravanan, K., Journal of Materials Science: Materials in Electronics vol **31**,issue 7 (2020) pp. 5710-5720
[13] Hessien, M., Da'na, E., Al-Amer, K. and Khalaf, M. M., Materials Research Express vol **6**,issue 8 (2019) pp. 085057
[14] Lopes de Almeida, W., Ferreira, N. S., Rodembusch, F. S. and Caldas de Sousa, V., Materials Chemistry and Physics vol **258**,issue (2021) pp. 123926
[15] Gong, W., Wang, G., Gong, Y., Zhao, L., Mo, L., Diao, H., Tian, H., Wang, W., Zong, J. and Wang, W., Solar Energy Materials and Solar Cells vol **234**,issue (2022) pp. 111404
[16] Singh, S., Kaur, H., Pathak, D. and Bedi, R., Dig J Nanomater Bios vol **6**,issue (2011) pp. 689-698
[17] Zhang, C., Tu, Q., Francis, L. F. and Kortshagen, U. R., Nanomaterials vol **12**,issue 3 (2022) pp. 565